

# Evaluation of high resolution snowpack simulations from global datasets and comparison with Sentinel-1 snow depth retrievals in the Sierra Nevada, USA

Laura Sourp<sup>1,2</sup>, Simon Gascoin<sup>1</sup>, Lionel Jarlan<sup>1</sup>, Vanessa Pedinotti<sup>2</sup>, Kat J. Bormann<sup>3</sup>, Mohammed Wassim Baba<sup>4</sup>

<sup>1</sup>Centre d'Etudes Spatiales de la Biosphère, CESBIO, CNES/CNRS/INRAE/IRD/Université Toulouse 3 Paul Sabatier, 31401 Toulouse, France

<sup>2</sup>MAGELLIUM, Ramonville Saint-Agne, 31520, France

<sup>3</sup>Airborne Snow Observatories, Inc., Mammoth Lakes, CA, United States

<sup>4</sup>Science, Applications & Climate Department, European Space Agency, Frascati 00044, Italy

*Correspondence to:* L. Sourp ([laurasourp@gmail.com](mailto:laurasourp@gmail.com))

**Abstract.** Spatial distribution of mountain snow water equivalent (SWE) is key information for water management. We implement a tool to simulate snowpack properties at high resolution (100 m) by using only global datasets of meteorology, land cover and elevation. The meteorological data are obtained from ERA5 which makes the method applicable in near real time (5 day latency). We evaluate the output using 49 SWE maps derived from airborne lidar surveys in the Sierra Nevada. We find a very good agreement at the catchment scale using uncalibrated lapse rates. Larger biases at the model grid scale are especially evident at high elevation but do not alter the catchment-scale snow mass accuracy. We additionally compare the simulated snow depth to Sentinel-1 retrievals and find a similar accuracy with respect to synchronous airborne lidar surveys. However, Sentinel-1 snow depth products are sparse and often masked during the melt season, whereas ERA5-SnowModel provides spatially and temporally continuous SWE.

## 1 Introduction

Many populated regions with dry summers and wet winters depend on mountain snow for water supply (Mankin et al., 2015; Sturm et al., 2017; Viviroli et al., 2020). Understanding the catchment scale seasonal snow storage before and during the melt season is key to optimizing water use between hydropower production, crop irrigation and freshwater supply. In addition, an accurate prediction of the timing and magnitude of the snowmelt runoff is bound by our ability to characterize the spatial distribution of mountain snow before the melt season (Freudiger et al., 2017).

28 Despite its hydrological significance, the snow water equivalent (SWE) remains poorly monitored in many mountain regions  
29 especially outside North America and Europe. In situ measurements are often too sparse considering the spatial variability of  
30 mountain snow (Fayad et al., 2017). To cope with this issue, airborne measurement campaigns are now routinely used in the  
31 western USA to measure snow depth but their cost remains prohibitive in other regions (Painter et al., 2016). Meanwhile,  
32 several approaches have emerged to retrieve mountain snow depth from satellite remote sensing (e.g. Pléiades, ICESat-2 and  
33 Sentinel-1). Pléiades very high resolution stereoscopic images can be used to generate snow depth images by differencing two  
34 digital elevation models. However, this approach is limited to small regions (Marti et al., 2016) ICESat-2 lidar altimetry has  
35 the potential to provide snow depth data at global scale but with a sparse sampling (Deschamps-Berger et al., 2023).  
36 Sentinel-1 has been used to derive snow depth at 1 km resolution in the northern hemisphere (Lievens et al., 2019), and 500 m  
37 over the European Alps (Lievens et al., 2022). This method, which is based on an empirical change detection method applied  
38 to the cross-polarization ratio, is limited to dry snow conditions and therefore does not allow monitoring of the snowpack  
39 during the melt season. However, it offers a global and spatially continuous coverage which is a key advantage with respect  
40 to the other approaches. All the above remote sensing approaches require an estimation of snow density to obtain the SWE,  
41 but it has been established that snow depth explains most of the SWE variance (Guyennon et al., 2019; López-Moreno et al.,  
42 2013; Sturm et al., 2010; Bormann et al., 2013).

43  
44 Another approach to estimating mountain SWE distribution is to use a snowpack model, but the challenge then lies with  
45 obtaining accurate meteorological forcing (Günther et al., 2019; Raleigh et al., 2016). To cope with the lack or sparsity of in  
46 situ meteorological measurements, one solution is to use atmospheric model outputs as forcing data. In particular, climate  
47 reanalyses can provide long term hourly meteorological data at global scale. Climate reanalyses are also becoming increasingly  
48 accurate (Hersbach et al., 2020) with advances in atmospheric and land surface modeling and the assimilation of a growing  
49 dataset of in situ and remote sensing observations. These reanalyses have also seen notable progress in recent years in terms  
50 of latency. For example, the preliminary ERA5 reanalysis provided by the European Centre for Medium-Range Weather  
51 Forecasts has a short latency of 5 days (whereas it was 2–3 months with the previous ERA-Interim). This preliminary product  
52 only rarely deviates from the fully quality-checked final product that is released 2 months later (Hersbach et al., 2020). This  
53 timely product can fulfill the need for up-to-date meteorological forcing information. However, reanalyses cannot be used  
54 directly to force a mountain snowpack model because the grid cell size is too coarse (approximately 30 - 50 kilometers for  
55 ERA5 and MERRA-2 respectively), which creates large biases in the computed SWE (Wrzesien et al., 2019; Liu et al., 2022).

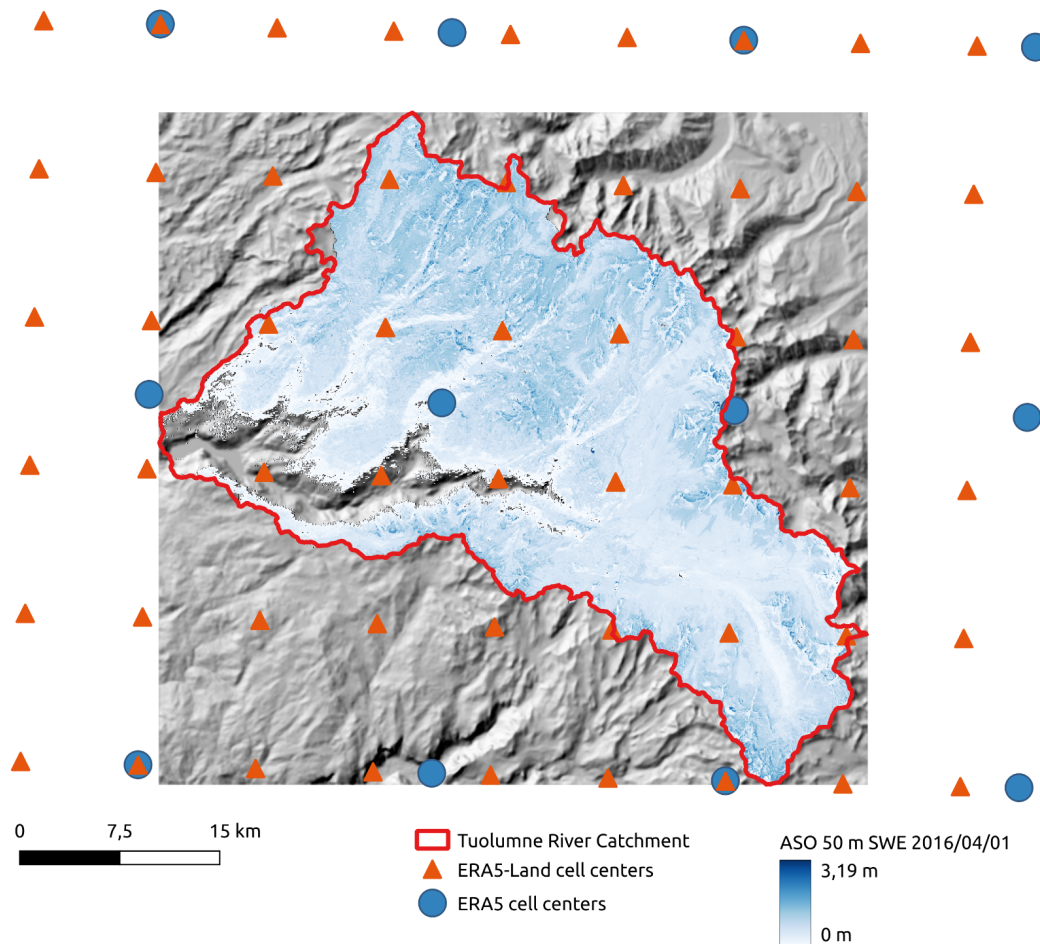
56  
57 To address the mismatch in spatial resolution between reanalyses datasets and snow distribution, previous studies used  
58 downscaling algorithms based on a digital elevation model before running a snowpack model on a finer grid (Armstrong et al.,  
59 2018; Baba et al., 2018; Billecocq et al., 2023; Mernild et al., 2017; Weber et al., 2021). This approach enables estimation of  
60 high resolution SWE and snow depth without ground data. For example, Mernild et al. (2017) and Baba et al. (2018) studied  
61 the snowpack properties over large and ungauged regions in the Andes and the High Atlas mountain ranges using the

62 MicroMet/SnowModel package (Liston et al., 2020; Liston and Elder, 2006a, b). The evaluation of these simulations relied on  
63 in situ observations or remote sensing snow cover area. Weber et al. (2021) used 10 years of snow depth measurements from  
64 two automatic weather stations to assess their simulations in the Research Catchment Zugspitze (12 km<sup>2</sup>). Mernild et al. (2017)  
65 used 13 years of MODIS data over the Andes Cordillera (~16 million km<sup>2</sup>) along with 4 km grid maps of snow depth that were  
66 reconstructed from in situ observations. Baba et al. (2018) used 18 years of MODIS data to assess simulations in the High  
67 Atlas of Morocco, snow depth at a single automatic weather station, precipitation at three meteorological stations and river  
68 discharge of the Ourika catchment (503 km<sup>2</sup>). However, in situ data are sparse and MODIS snow cover area does not allow a  
69 thorough evaluation of the model ability to capture snow mass across the landscape.

70

71 In this study, we focus on the Tuolumne River catchment in the Sierra Nevada, USA (Figure 1). Since 2013, this site has been  
72 regularly surveyed by the Airborne Snow Observatory (ASO) to determine snow depth and SWE. The ASO dataset on the  
73 Tuolumne catchment is the densest time series of high resolution snow depth (3 m) and SWE (50m) maps publicly available  
74 at this scale (1100 km<sup>2</sup>) in the world. The dataset contains 49 surveys and spans several years with contrasted climatic  
75 conditions including California's most severe drought in the last 1200 years during 2012-2014 (Griffin & Anchukaitis, 2014)  
76 and the "snowpocalypse" 2016–2017 winter which was characterized by near-record snow accumulation (Painter et al., 2017).  
77 We leverage this observational dataset to evaluate a new processing pipeline which generates 100 m resolution SWE and snow  
78 depth estimates from ERA5 or ERA5-Land. This pipeline, inspired by previous works (Baba et al., 2018; Mernild et al., 2017)  
79 is a wrapper around MicroMet/SnowModel code. It was designed to work with global meteorological forcing datasets. As  
80 such, the workflow can generate high resolution snow cover simulations in any region of interest across the globe from 1940  
81 up to present, with any resolution between 1 m and 200 m (Liston and Elder, 2006b). Furthermore, we compare the output of  
82 this pipeline with the more direct approach of Sentinel-1 snow depth on dates matching the ASO measurements.

83



85

86 **Figure 1: Map representing the SWE variability measured by ASO, along with ERA5 and ERA5-Land cells centers**  
 87 **and the Tuolumne River catchment border overlaying the DEM hillshade.**

## 88 2 Data and Methods

### 89 2.1 Data

90 We used two reanalyses in this study, ERA5 and ERA5-Land. ERA5 is a reanalysis of the global climate and weather since  
 91 1940, with a  $0.25^\circ$  resolution (approximately 30 km). It provides hourly atmospheric, oceanic and land-surface variables  
 92 computed with a global model and improved by the assimilation of multiple in situ and remote sensing datasets (Hersbach et  
 93 al., 2020). ERA5-Land is produced by recomputing ERA5 land variables at finer resolution using a downscaled meteorological  
 94 forcing (Muñoz Sabater, 2019). It delivers these variables on a global scale at a  $0.1^\circ$  resolution, from 1950 to this day. As  
 95 mentioned above, preliminary versions of ERA5 and ERA5-Land are distributed with a short latency of 5 days. These datasets

96 are freely available from the Copernicus Climate Change Service (C3S) and can be queried via their application programming  
97 interface (with tutorials that can be found on their website : Retrieving data — Climate Data Store Toolbox 1.1.5  
98 documentation)

99 . We focused on ERA5 here as we found that it yielded slightly better results than MERRA-2 in a previous case study using  
100 the same approach (Baba et al., 2021). In addition, the latency of MERRA-2 is 3 weeks which may be too long for operational  
101 water resources applications. To run the model (see section 2.2.1 ), we also used the 30 m Copernicus Digital Elevation  
102 Model (DEM) (Copernicus Digital Elevation Model, 2023) and the 100 m Copernicus Land Cover (Buchhorn et al., 2020).

103

104 We obtained Sentinel-1 snow depth between 2016 and 2019 from the C-SNOW repository (C-SNOW). Sentinel-1 C-band  
105 backscatter observations were used to derive ~1 km resolution snow depth, using an empirical change detection (Lievens et  
106 al., 2019). This product has a revisit time of approximately 3 days over the Tuolumne River catchment during winter but  
107 provides almost no data in spring because the algorithm is considered to be invalid when the snowpack contains liquid water.  
108 When the snowpack is wet, there is a larger absorption and reflection of the microwave signal emitted by Sentinel-1 which  
109 greatly decreases the performances of the C-SNOW algorithm (Lievens et al., 2019; Tsai et al., 2019).

110

111 For the evaluation of model outputs and Sentinel-1 products, we used 49 SWE and snow depth maps collected between 2013  
112 and 2019 by the ASO. The ASO acquires hyperspectral data for snow albedo and lidar data for snow depth and computes SWE  
113 as a derived product (Painter et al., 2016). Snow depth is available with a 3 m resolution while SWE has 50 m resolution. The  
114 reported accuracy on the 3 m snow depth products is 0.08 m (Painter et al., 2016) and from spatially intensive sampling, the  
115 reported accuracy for the 50 m snow depth products is < 0.01 m (Painter et al., 2016, Figure 15). There are no published  
116 references for the 50 m SWE product. However, Rayleigh & Small (2017) estimated an uncertainty in modeled density of 48  
117 kg/m<sup>3</sup> in the Tuolumne basin. This uncertainty can be regarded as a conservative estimate as in situ measurements of snow  
118 density are also used by the ASO to adjust their density model (Painter et al., 2016). Therefore, for a 1 m deep snowpack and  
119 an uncertainty in snow density of 50 kg/m<sup>3</sup> , we estimate the uncertainty of the 50 m SWE products to be 0.05 m  
120 w.e (meters of water equivalent) .

## 121 **2.2 Methods**

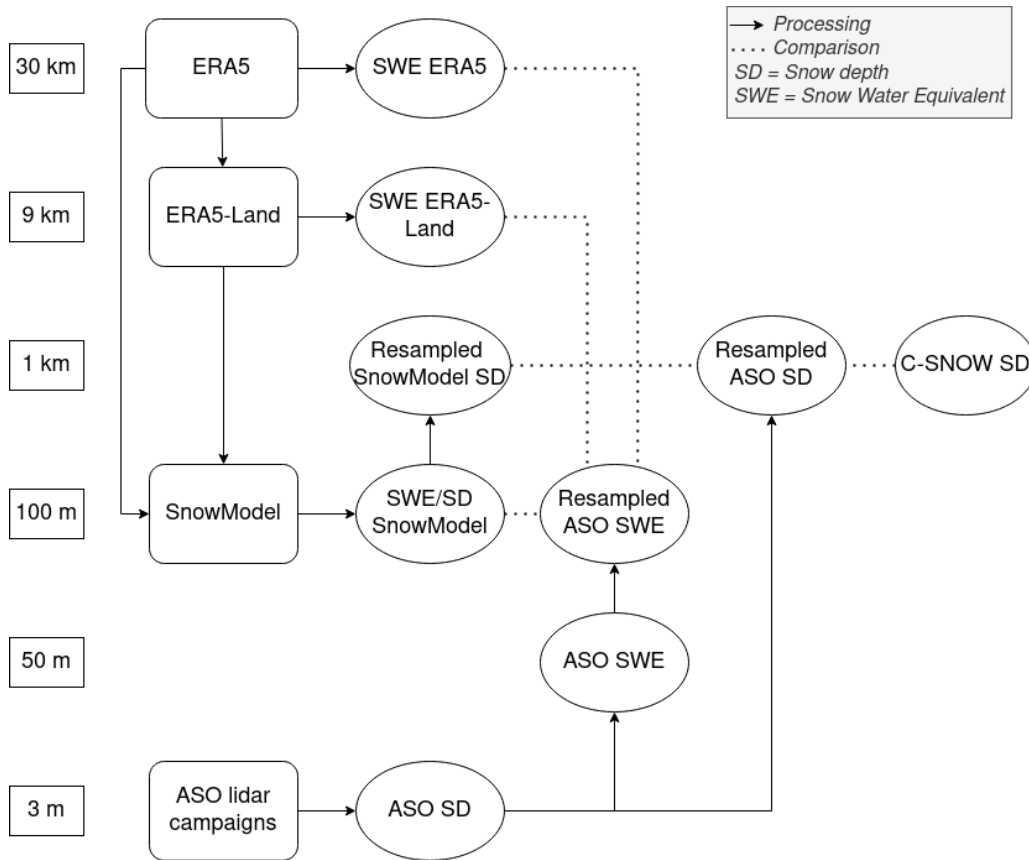
### 122 **2.2.1 SnowModel**

123 SnowModel is designed to simulate snow evolution on a high resolution grid (1 m to 200 m increments) and a time step from  
124 1 min to 1 day (Liston et al., 2020; Liston and Elder, 2006a). It is separated into four submodels: i) MicroMet redistributes  
125 meteorological forcings (air temperature, relative humidity, wind speed and direction, precipitation, solar radiation, long wave  
126 radiation, and surface pressure) to the target simulation grid (Liston and Elder, 2006b). ii) EnBal computes the snow surface  
127 energy balance, iii) SnowPack computes the snow density and snow depth and iv) SnowTran-3D computes the blowing snow

128 sublimation and snow redistribution due to wind transport (Liston et al., 2007). SnowModel accounts for the vegetation effects  
 129 on the snow cover such as coniferous forests or grassland to the grid cell vegetation type. MicroMet was originally designed  
 130 to interpolate station data on a regular grid. Here, a climate reanalysis grid cell is considered as a virtual station located at the  
 131 grid cell center.

132

133 **2.2.2 Model input**



134

135 **Figure 2: Summary of the different data sources, with their spatial resolutions. Arrows represent a process and the**  
 136 **dotted lines the comparison between different data.**

137

138 We developed a tool to automatically prepare SnowModel input files from ERA5 and ERA5-Land data and run the simulations.  
 139 This tool uses a DEM of the region of interest as an input along with the start and end of the simulation period. We let the  
 140 user specify the DEM because it is used to define the model grid, which is the main control of the computation time. Here we  
 141 used the 30 m Copernicus orthometric DEM that we extracted and resampled to a WGS84 UTM 11N grid at 100 m resolution  
 142 using the bilinear method over a region covering the Tuolumne River catchment. The simulation period was set to September

143 2012-August 2019, and spans seven years of snowpack dynamics. Using the Climate Data Store Application Program  
144 Interface, our tool downloads ERA5 or ERA5-Land hourly meteorological data ( 2 m temperature, 2 m dew point temperature,  
145 precipitation, 10 m wind eastward and northward component) over the region of interest given by the DEM bounding box  
146 extended to the adjacent ERA5/ERA5-Land neighbouring cells (~30km/11km respectively). Once downloaded, the  
147 meteorological data are processed to match SnowModel/MicroMet input format and  
148 units. ERA5-Land precipitation is provided as daily cumulative values and is therefore converted to hourly precipitation rate.  
149 Wind components (u,v) are converted into wind speed and direction (0-360°N). The dew point temperature is converted into  
150 relative humidity using Buck's equation (Buck, 1981), the same equation that is used in MicroMet. The elevations of  
151 ERA5/ERA5-Land cells are determined from the global geopotential file that is first interpolated on the model grid with a  
152 bilinear algorithm. The tool also resamples the Copernicus land cover map on the model grid using the mode resampling  
153 algorithm (GDAL/OGR contributors, 2024). We built a correspondence table to remap the Copernicus land cover classes to  
154 the SnowModel land cover classification (see Table A1 in appendix). We set all SnowModel parameters (the curvature length  
155 scale, curvature and wind slope weights, minimum wind speed, precipitations schemes for downscaling or for rain-snow  
156 fractions, subcanopy radiations schemes, various thresholds for wind transport calculations) to the default values (see the  
157 parameter file snowmodel.par in the code availability section) . A simple parametrization of the albedo is used with a constant  
158 value 0.8 in dry condition, whereas albedo values for melting snow cover are set according to land covers (Liston et al., 2020).  
159 We used the default monthly temperature lapse rates and precipitation factors which adjust the precipitation values to the  
160 elevation of the model grid. This tool is implemented in Python. The source code and a more detailed documentation is  
161 available at (code availability section).

### 162 **2.2.3 Comparison with ASO SWE**

163 We resampled the ASO SWE (n=49 surveys) to the model grid which has a resolution (100 m). The resampling was done  
164 using the weighted average of all valid contributing pixels (GDAL/OGR contributors, 2024). We also created a validity mask  
165 to select cells in the Tuolumne River catchment that were always observed by the ASO during this period (some regions were  
166 not always available, representing 2.5% of the catchment area). ASO data and ERA-SnowModel outputs were averaged over  
167 the valid cells to compute the temporal evolution of the catchment-mean SWE. Then, we analyzed the spatially distributed  
168 residuals on the catchment for each observation date of a dry year (2014-2015), a wet year (2016-2017) and an average year  
169 (2015-2016). We used the validity-masked SWE maps to subtract the ASO observations from the ERA-SnowModel output. A  
170 positive bias means the simulated SWE is larger than the observations.

171  
172 Additionally, we extracted ERA5 and ERA5-Land daily SWE over the Tuolumne River catchment and computed the  
173 catchment scale SWE using an area weighted average (i.e. each SWE value was weighted by the fraction of the grid cell area  
174 within the catchment). Since these SWE products have a very coarse resolution of approximately 31 and 9 km ( Fig. 1, Fig. 2),  
175 we did not use them to analyze the residuals distribution as above.

## 176 **2.2.4 Comparison with Sentinel-1 snow depth**

177 Over the entire study period, we identified three matchup dates for which we have both ASO and Sentinel-1 snow depth  
178 observations with a minimum coverage of 60% of the catchment area. On these dates, the snow depths given by ASO, Sentinel-  
179 1 and ERA-SnowModel were resampled to a common 1 km UTM grid. We applied another validity mask for the cells where  
180 the snow depth is not always available to all three snow depth datasets (here representing 8.5% of missing data in the  
181 catchment). The missing values in the 3 m resolution ASO dataset are propagated at the 1 km resolution validity mask. This  
182 decreases the number of observations but ensures that the resampled 1 km snow depths maps are not biased by the spatial  
183 distribution of non-valid pixels in the 3 m ASO snow depth dataset. We computed the distributed residuals by subtracting  
184 the ASO snow depth from both SnowModel simulations and Sentinel-1 data. For each date, we averaged the residuals to  
185 compute the mean bias, and we computed the standard deviation of the error. We also computed the RMSE over the catchment  
186 for each date .

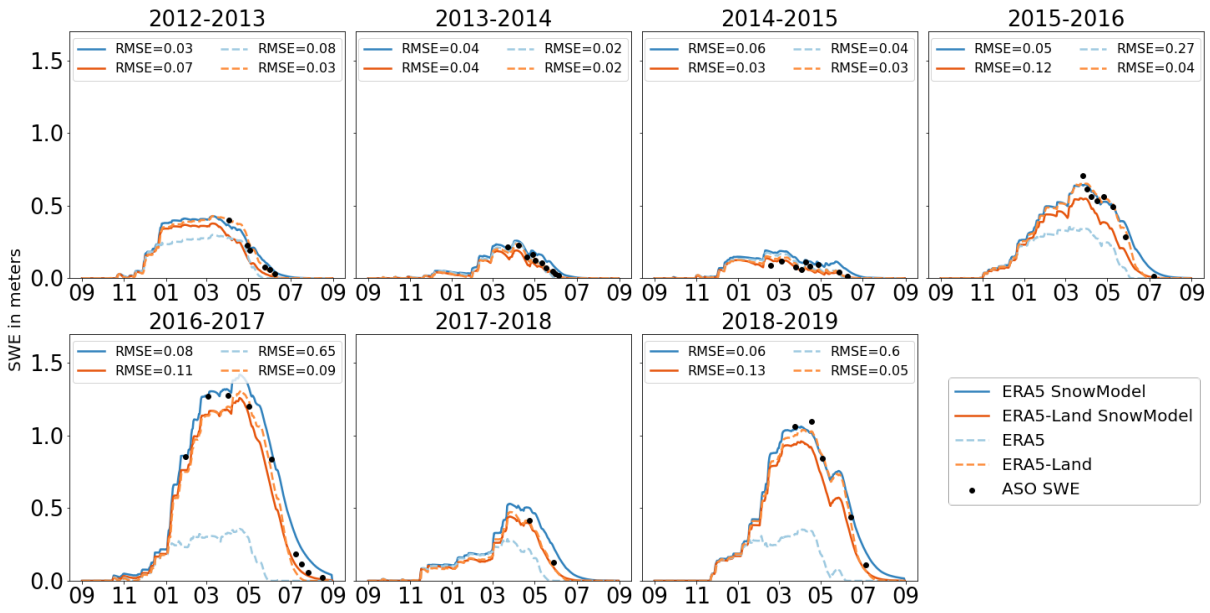
## 187 **3 Results**

### 188 **3.1 Comparison with ASO SWE**

189 Figure 3 shows the temporal evolution of the catchment scale SWE from ASO observations and SnowModel simulations  
190 forced with ERA5 and ERA5-Land. There is a very good agreement between the observations and both simulations, with an  
191 overall correlation of 0.99 for both ERA5 and ERA5-Land SnowModel simulations (with 49 observation dates). First, both  
192 simulations capture the large interannual variability of SWE in the Tuolumne River catchment during the study period. The  
193 observed annual peak SWE ranges from 0.11 m in 2015 to 1.27 m in 2017 while the SnowModel simulations yield from 0.17  
194 m to 1.19 m with ERA5 and from 0.12 m to 1.24 m with ERA5-Land during the same years (but at different dates). In addition,  
195 the model is reproducing the seasonal evolution of SWE with an annual RMSE ranging from 0.03 m to 0.13 m. The catchment  
196 scale SWE accumulation in the ERA5-SnowModel simulations is well captured. We note an underestimation of the snow  
197 ablation rates in late spring, which causing a delay from a few days (2013) to one month approximately (2019) in the date of  
198 complete melt out. This issue is mostly evident in 2016-2017 since the ablation rates are insufficient to reach the complete  
199 removal of the snowpack in August as observed by the ASO. Interestingly, we also note that ERA5-Land without resampling  
200 almost always reports the lowest RMSE at the catchment scale, though at 0.1° the distribution of the snow is not well  
201 represented.

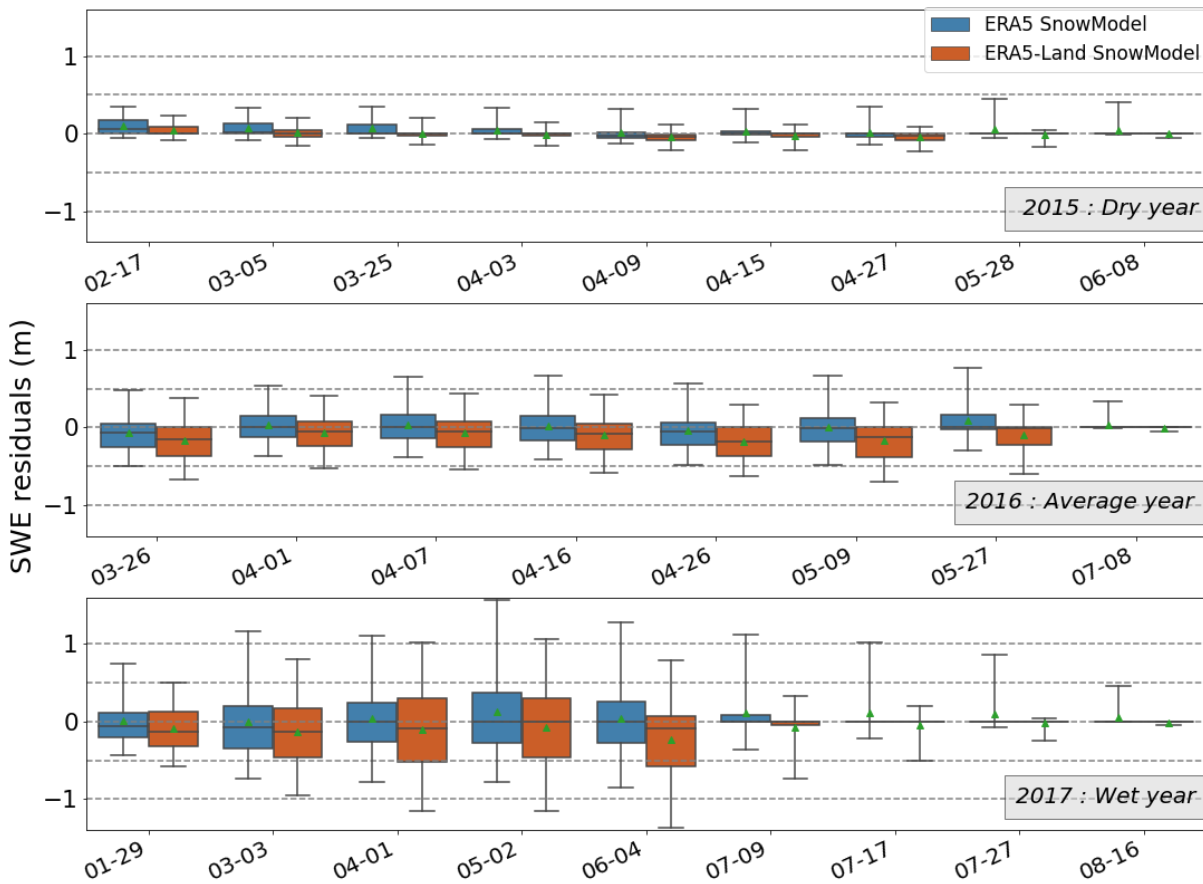
202





203  
204 **Figure 3: Temporal evolution of the Tuolumne river catchment SWE for seven hydrological years from 2012 to 2019.**  
205 **The legend indicates the RMSE between the simulated SWE and the ASO SWE for each year.**

206  
207 To go beyond this coarse catchment scale diagnostic (1100 km<sup>2</sup>), we also analyze the distribution of the residuals at the pixel  
208 scale (0.01 km<sup>2</sup>). We computed a map of RMSE using all the 49 validation dates we have between 2013 and 2019. 10% of the  
209 cells in this map have a RMSE above 0.5 m w.e.. Figure 4 shows the distribution of the residuals for every date with ASO  
210 observations for three contrasted hydrological years. The spread of the residuals are shown with the interquartile (i.e., the  
211 difference between the 25 and 75th percentiles) inside the colored boxes, and with the 5-95th percentiles inside the whiskers.  
212 This figure indicates that the spread of the residuals increases with the mean SWE depth. For the dry year, the interquartiles  
213 of SnowModel SWE residuals for ERA5 and ERA5-Land do not exceed 0.17 m and 0.09 m w.e. respectively. For the average  
214 year, the interquartiles reach 0.31 m and 0.38 m w.e. and for the wet year 2017, they peak respectively at 0.64 and 0.82 m  
215 w.e.



217

218

219

220

221

222

223

224

225

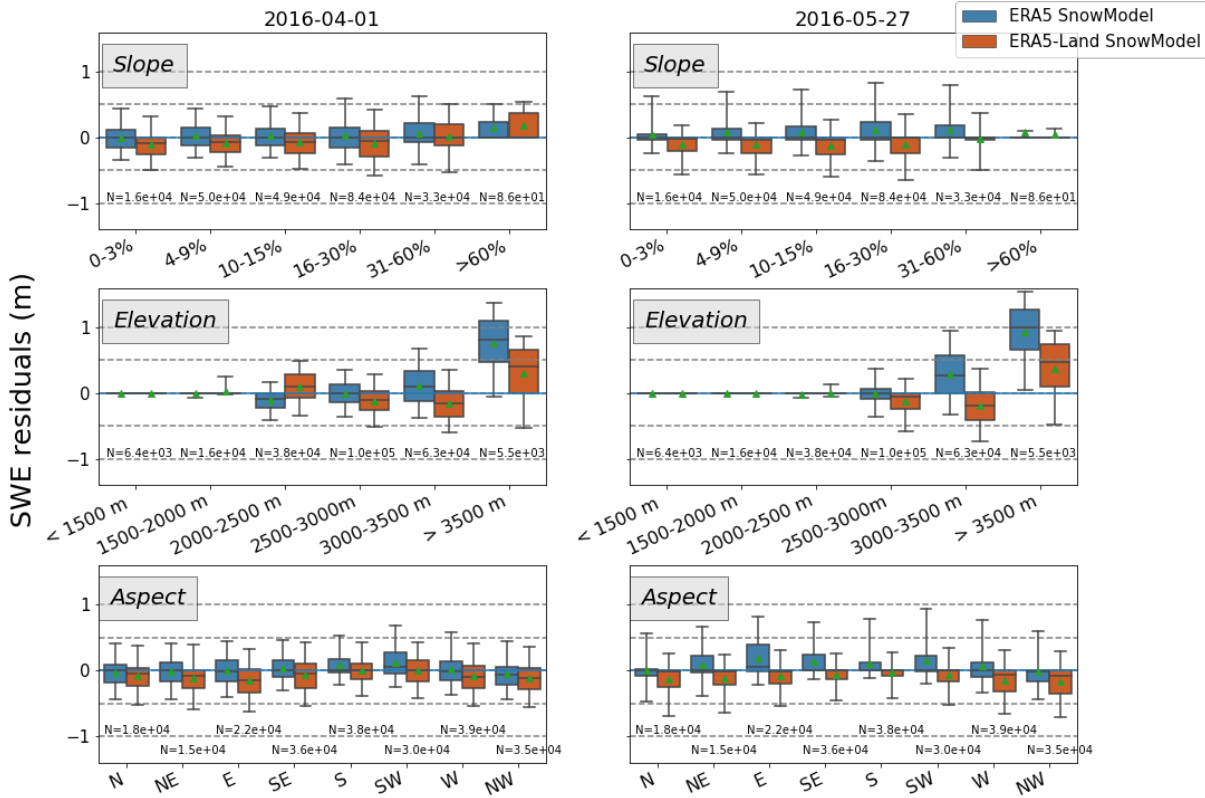
226

227

228

**Figure 4: Distribution of the residuals between the SnowModel simulated SWE and the ASO SWE at 100 m resolution in the Tuolumne river catchment (in m w.e.) for three contrasted hydrological years. Filled boxes represent the interquartile range, the whiskers show the 5-95 percentiles, the line in each box represents the median of the distribution, and the green triangle shows the mean.**

Figure 5 shows the distribution of the residuals for two dates (2016-04-01 and 2016-05-27) by slope, elevation and aspect. We aimed to distinguish the model performance in terms of accumulation and ablation processes to better separate the sources of uncertainties in future studies. Therefore we selected a date before the melting season (April 01 2016) and a date near the end of the melting season (May 27 2016). The interquartile of the error distribution never exceeds 0.41 m.w.e. in slope or aspect categories but peaks at 0.67 m.w.e. in the highest elevation band the 1st of April for the simulations forced with ERA5-Land.

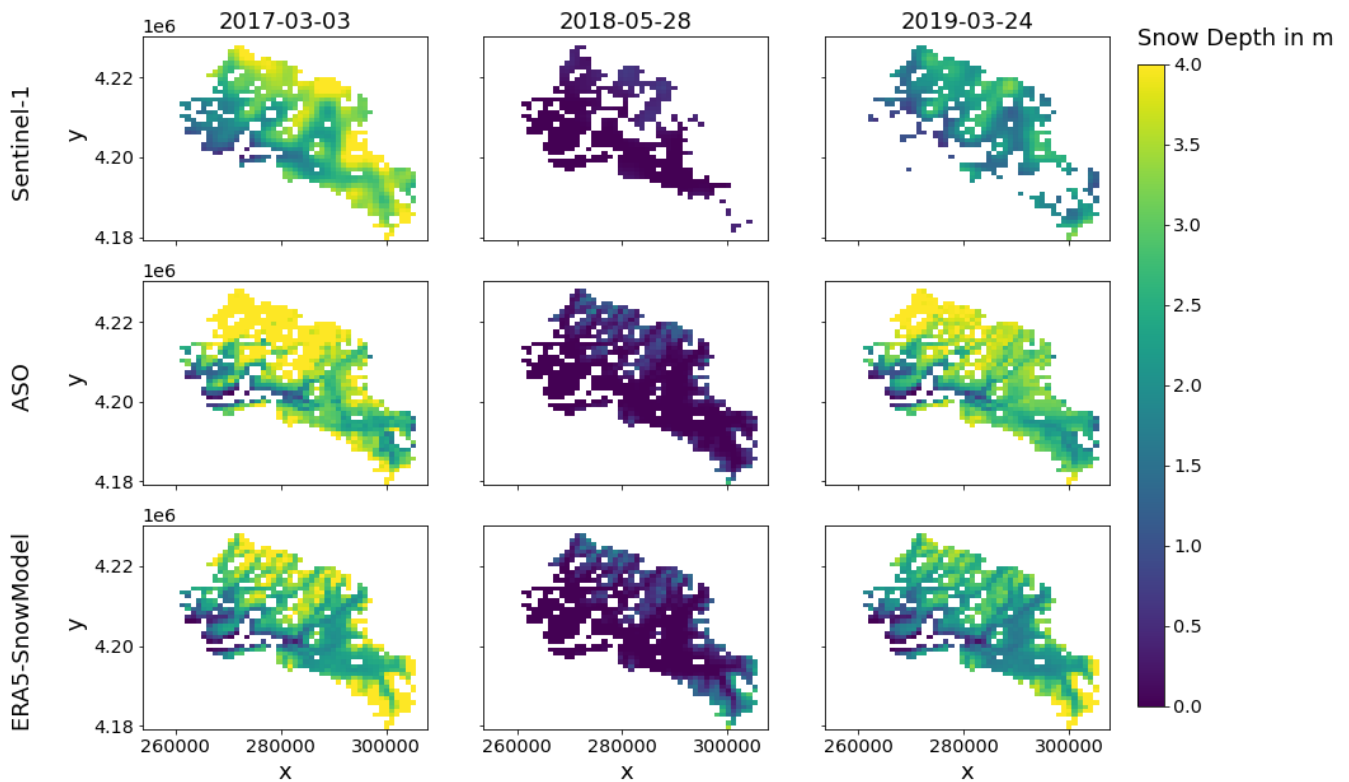


229

230 **Figure 5: Distribution of the residuals between the SnowModel simulated SWE and the ASO SWE at 100 m resolution**  
 231 **in the Tuolumne river catchment (in m w.e.) on the 1st of April 2016 (left) and the 27th of May (right), stratified by**  
 232 **slope (in percent), elevation (in m a.s.l.) and aspect (in degrees from north). Whiskers show the 5-95 percentile, the line**  
 233 **in each box represents the median of the distribution and the green triangle shows the mean. Slope, elevation and**  
 234 **aspects have been calculated using the DEM at 100 m resolution.**

235 **3.2 Comparison with Sentinel-1 snow depth**

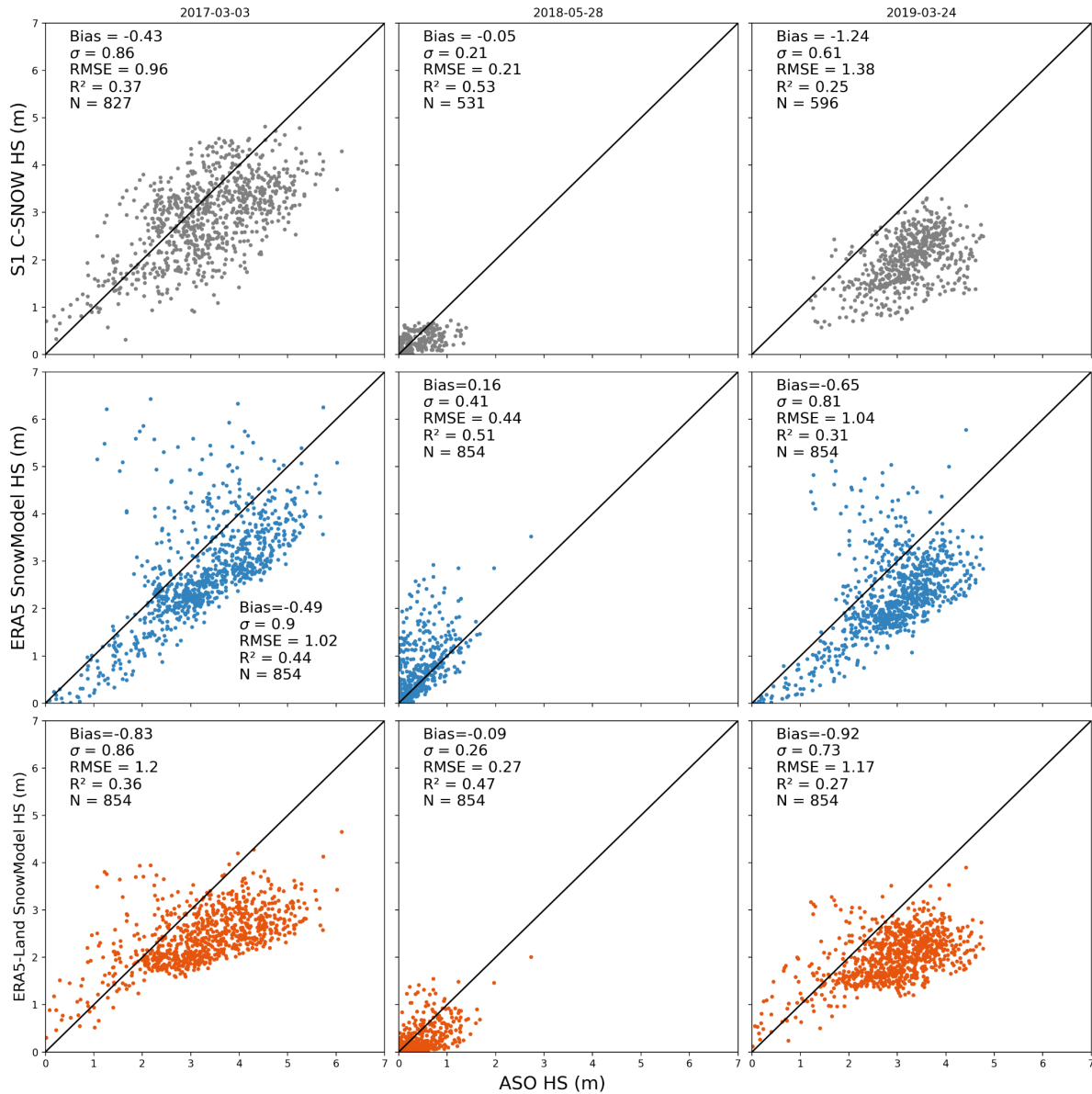
236 Between 2016 and 2019, there are three dates for which we have both Sentinel-1 and ASO snow depth data. Figure 6 presents  
 237 snow depth maps on the Tuolumne River catchment at 1 km resolution with Sentinel-1, ASO and ERA5-SnowModel data.  
 238 Some pixels are not always observed with ASO data and these missing values are propagated at 1 km resolution (if there is at  
 239 least one missing value among the contributing pixels, a missing value is attributed to the target 1 km cell). The same mask is  
 240 applied on the SnowModel simulations and Sentinel-1 data. Additional missing values are observed in the Sentinel-1 snow  
 241 depth maps. Therefore, the statistics of Figure 7 are not computed on the exact same area. We chose to take all possible data  
 242 into account.



243  
244 **Figure 6: Snow depth maps at 1 km resolution with Sentinel-1, ASO and ERA-SnowModel data.**

245  
246 Figure 7 shows the Sentinel-1 observed and SnowModel simulated snow depth compared to the ASO observed snow depth,  
247 resampled to a 1 km resolution. On the 2017-03-03, Sentinel-1 has the lower bias (-0.43 m), standard deviation (0.86 m) and  
248 RMSE (0.96 m). These statistics are close to the ERA5-SnowModel simulations (respectively -0.49 m, 0.9 m, 1.02 m) while  
249 ERA5-Land-SnowModel simulations have a greater bias (-0.83 m) and RMSE (1.2 m) with a comparable standard deviation  
250 (0.86 m). On the second date, the 2018-05-01, Sentinel-1 still performs the best with a bias of -0.05 m, and standard deviation  
251 and RMSE both equals to 0.21 m . On this date, ERA5-Land-SnowModel simulations are similar to Sentinel-1 with a  
252 bias of -0.09 m, standard deviation of 0.26 m and RMSE of 0.27 m; while ERA5-SnowModel simulations underperform with  
253 a 0.16 m bias, a 0.41 m standard deviation and a 0.44 m RMSE.. Finally on the 2019-03-24, the closer data to the ASO snow  
254 depths seems to be the ERA5-SnowModel simulations with an bias of -0.65 m, a standard deviation of 0.81 m and an RMSE  
255 of 1.04 m. Sentinel-1 data have the highest bias (-1.24 m) and RMSE (1.38 m), but the lowest standard deviation (0.61  
256 m) . ERA5-Land-SnowModel simulations also have a high bias (-0.92 m) and RMSE (1.17 m), with a standard deviation of  
257 0.73 m. We see an underestimation of the snow depth above 2 meters with Sentinel-1 in 2017 and 2019, which is very clear  
258 for 2019 when the mean bias is the highest with a relatively low standard deviation. In 2018, both the ASO and Sentinel-1  
259 observed really low snow depths (<1 m) but there is still a negative bias (-0.05 m) in the Sentinel snow depth distribution .

260 With the ERA5 SnowModel simulations, most of the distribution is centered around a negative bias that is underestimating  
 261 the snow depth in 2017 and 2019. We note several cells with a high positive error. In 2018, the situation is reversed : most of  
 262 the snow depth estimated with ERA5 SnowModel are overestimated. Finally, the simulations with ERA5-Land seem to cap at  
 263 4 meters of snow depth in 2017 and 2019, with a declining accuracy with the ASO snow depth starting at 2 m. In 2018, the  
 264 ERA5-Land SnowModel simulations are mostly underestimating snow depths.  
 265



266

267 **Figure 7: Scatter plots representing the observed and SnowModel simulated snow depth data as a function of ASO**  
268 **snow depth data, with a one to one line in black. All data are resampled at 1 km resolution. N is the number of values**  
269 **in each plot.**

270

## 271 **4 Discussion**

272

273 Downscaling ERA5 forcing is critical to obtain realistic SWE in the Tuolumne catchment and is sufficient to remove the strong  
274 negative bias that is otherwise present in the original ERA5 SWE (Fig 3). The use of this pipeline for long simulation periods  
275 could also bypass the discontinuities in the ERA5 SWE (Urraca and Gobron, 2023) which are caused by a snow capping in  
276 the data assimilation code and the arrival of new snow depth data available for assimilation. The main effect of the downscaling  
277 is a better representation of the air temperature distribution and therefore a better representation of the solid precipitation  
278 fraction. Then, the performance of the SnowModel simulated SWE largely relies on ERA5 precipitation. Our results suggest  
279 that the winter precipitation is well represented by ERA5 over the Sierra Nevada, in agreement with previous studies  
280 highlighting the good performances of ERA5 precipitation especially in extratropical regions (Lavers et al., 2022). We find an  
281 overestimation of snow accumulation in high elevation which occurs only above 3000 m asl. In the study domain, the maximum  
282 elevation of ERA5 and ERA5-Land grid cells are 2654 m and 3100 m respectively. Hence the overestimation shown in Figure  
283 5 is likely due to the extrapolation of ERA5 precipitation by MicroMet. MicroMet uses monthly coefficients to adjust  
284 precipitation with elevation. These coefficients were derived from a large precipitation gauge dataset in the Western North  
285 America including the Tuolumne river catchment (Liston and Elder, 2006b). As a result, they only represent a first order  
286 variation of precipitation with elevation and may introduce large biases only in areas whose fine scale elevation (i.e. at the  
287 scale of the 100 m grid) deviates substantially from the ERA5 grid cell elevation. A possible source of error in high elevation  
288 regions is the lack of gravitational transport in SnowModel. High elevation and steep slopes are prone to avalanches thereby  
289 reducing the accumulated snow in these areas during the winter season (Quéno et al., 2023). However, we did not find a clear  
290 correlation between the terrain slope and the model error (Fig. 5). Slopes above 15% have a slightly wider error distribution  
291 but the mean absolute biases remain below 0.10 m w.e for both simulations. We also verified the residuals distribution by  
292 average slope classes computed from a 3 m resolution slope raster (computed from the ASO snow-off lidar DEM) and found  
293 similar results (see Figure A2 of the appendix). Hence, we do not see clear evidence that the lack of gravitational transport is  
294 the main cause of the high elevation biases. Another significant source of uncertainty is related to the albedo parameterization  
295 in SnowModel. The deposition of light absorbing particles like dust can reduce albedo and therefore increase melt especially  
296 at high elevation (Skiles et al., 2018; Dumont et al., 2020). This might explain the relative increase of the SWE bias between  
297 the 1st of April and the 27th of May at all elevations above 2500 m (Figure 5).

298

299 At catchment scale we do not find a clear difference between ERA5-SnowModel and ERA5-Land-SnowModel outputs. This  
300 suggests that the details of the downscaling scheme are not the primary factors of the simulation performance. However, there  
301 is a deviation between both simulations at high elevation. As shown in Figure 5, the downscaling of ERA5 creates a strictly  
302 increasing bias with elevation above 2500 m, whereas ERA5-Land creates a more complex bias that is negative between 2000  
303 m and 3000 m and becomes positive above 3500 m. This more complex bias distribution reflects the fact that the output of the  
304 ERA5-Land SnowModel pipeline is the result of two downscaling schemes (first ERA5 to ERA5-Land, then ERA5-Land to  
305 100 m using MicroMet, Fig. 2). ERA5-Land atmospheric variables are generated by linear interpolation of their ERA5  
306 counterparts. ERA5-Land air temperature and humidity are also adjusted using the grid cell elevation using a daily lapse rate  
307 derived from ERA5 lower troposphere temperature vertical profile (Dutra et al., 2020). This is similar to the MicroMet  
308 algorithm. Yet, there are several differences. In particular, the air temperature downscaling scheme in ERA5-Land is based on  
309 a daily environmental lapse rate derived from ERA5 lower troposphere temperature vertical profiles (Muñoz Sabater, 2019),  
310 whereas MicroMet lapse rates are fixed by month. Unlike ERA5-Land, MicroMet also adjusts the precipitation rates using a  
311 function of elevation (Liston and Elder, 2006b). This is the cause of the non-monotonic evolution of the SWE bias by elevation  
312 from ERA5-Land-SnowModel. In future applications we will favor ERA5 instead of ERA5-Land to avoid conflicting  
313 processes in the downscaling of atmospheric variables. It makes it easier to adjust the precipitation correction factors from  
314 local data. Using ERA5 is also more practical as it significantly reduces the download time, computing cost and memory usage  
315 of our pipeline.

316

317 In Figure 3, we note the very good performance of ERA5-Land SWE at catchment scale despite its coarse scale (9 km  
318 resolution). This result is in line with Muñoz-Sabater et al. (2021) who find better performances of ERA5-Land than ERA5  
319 between 1500 m and 3000 m a.s.l. because 68% of the Tuolumne River catchment is in this elevation band. Shao et al.  
320 (2022) found a similar accuracy of the ERA5-Land SWE dataset with an RMSE below 0.04 m w.e. in regions north of  
321 45°N. This evaluation was performed using point-scale in situ measurements over large flat regions and not in complex  
322 mountain terrain like the Tuolumne Basin where the high spatial variability of SWE makes such evaluation more challenging  
323 (Mortimer et al. 2024). Overall, the performance of ERA5-Land SWE needs to be consolidated in other regions and ideally  
324 over larger domains of mountainous areas. Previous studies suggested that a resolution below 500 m is required to properly  
325 simulate the snowpack distribution (Baba et al., 2019; Bair et al., 2023). In addition, ERA5-Land resolution does not meet the  
326 essential climate variable requirements set by the World Meteorological Organization for SWE (goal is 500 m resolution)  
327 (WMO e-Library, 2024).

328

329 Regarding Sentinel-1, Figure 7 suggests that the snow depth is well captured by the C-SNOW algorithm at 1 km resolution.  
330 Although we are interested in SWE and not snow depth, the ASO program has shown that useful SWE products can be derived  
331 from remotely sensed snow depth when combined with in situ measurements and modeled snow density (Painter et al.,  
332 2016). Figure 7 shows that Sentinel-1 snow depth dataset agrees moderately with the spatial variability inside the catchment,

333 although we note a slight underestimation for all three dates before the melting period (2017 and 2019) and after it (2018).  
334 There is no clear pattern in the errors that emerge from these three dates. Other studies highlighted that the C-SNOW algorithm  
335 is not adapted to retrieve snow depth of shallower snowpack (<1.5 m) (Broxton et al., 2024; Hoppinen et al., 2024) which could  
336 be a significant obstacle for an operational use of this product. The modeling approach with ERA-5 (Land) and SnowModel  
337 yields similar performances in terms of snow depth as the C-SNOW product on the same dates. However, two patterns appear  
338 on Figure 7 for these approaches. i) The simulations with ERA5 and SnowModel are mostly centered around a negative bias  
339 constant with the observed snow depth before the melting period (2017 and 2019), probably representing a small negative bias  
340 in the ERA5 precipitation. ii) The simulations with ERA5-Land SnowModel seem to cap at 4 m which could be the result of  
341 the two consecutive downscalings in the precipitations : the combination of an underestimation of ERA5 precipitation and its  
342 downscaling, plus the limitation of the elevation difference between ERA5-Land stations and the DEM so the MicroMet  
343 precipitation factor cannot enhance enough the high resolution precipitations. Overall, the key difference in the Tuolumne  
344 catchment is that the model provides temporally continuous SWE, snow depth and other relevant variables like snowmelt  
345 runoff, whereas C-SNOW snow depth products are temporally sparse and often masked during the melt season.  
346

347 Our study has several limitations. Despite the large amount of data that were used for this study, our analysis is biased towards  
348 the melt season since most of the ASO surveys were performed during the melt season for operational purposes. As a  
349 consequence, the evaluation of the Sentinel-1 snow depth is limited to three dates only. In addition, we used ASO SWE which  
350 is not a direct observation but a combination of accurate snow depth measurements and modeled snow density. Previous work  
351 has shown that SWE variability is mostly driven by the snow depth variability (López-Moreno et al., 2013; Sturm et al., 2010).  
352 Another limitation is the fact that ERA5 meteorological forcings may not be homogeneous across the globe due to the uneven  
353 distribution of the assimilated observations. In addition, MicroMet precipitation correction coefficients were obtained from a  
354 large region covering the study area, hence they may not be applicable in other regions. Therefore, we cannot generalize our  
355 results to other regions. However, the increasing weight of global satellite observations in ERA5 over time suggests that ERA5  
356 performances should be more spatially homogeneous in the recent and upcoming years. As a consequence, ERA5 uncertainty  
357 varies with time since more and more data are available for data assimilation (Bell et al., 2021). This could be a limitation to  
358 compute trends over large periods (Bengtsson et al., 2004).  
359

360 However these errors have a low impact at the catchment scale and we can conclude that ERA5-SnowModel is promising for  
361 water resources applications. This pipeline can be used to simulate SWE in near real time without the need of in situ  
362 measurements. The development of a parallel version of SnowModel opens the door to continental scale applications (Mower  
363 et al., 2023).



## 364 **5 Conclusion**

365 We have evaluated a pipeline to simulate the snowpack in mountainous catchment from global datasets only. This tool is based  
366 on Copernicus land cover and DEM, ERA5 (or ERA5-Land) and SnowModel. It uses SnowModel/MicroMet to downscale  
367 meteorological variables from ERA5 before computing accumulation and ablation processes using other SnowModel  
368 submodels. It can generate daily gridded snow water equivalent over any region and any period of interest since 1940. Based  
369 on 49 reference SWE surveys spanning seven contrasted hydrological years, we find that the ERA5-SnowModel combination  
370 simulates well the SWE at the scale of the Tuolumne river catchment, with RMSE of 0.06 m (and 0.08 m with ERA5-Land)  
371 and correlation of 0.99 (with both datasets). The SWE is also well simulated by elevation bands, except in the highest elevation  
372 band where unrealistic SWE values were simulated. Between ERA5 and ERA5-Land, ERA5 is more convenient to use  
373 especially because it requires less computing resources. Using the near -real- time release of ERA5 allows the simulation  
374 of SWE with a 5 day latency. This makes this method usable in operational context and competitive with a satellite-based  
375 approach. In particular, we found that it simulates the snow depth as well as the C-SNOW products derived from Sentinel-1,  
376 which is only available during dry snow conditions.

377  
378 Our study focused on a single catchment due to the availability of the ASO SWE products. However, ERA5 skills may vary  
379 geographically and temporally due to the heterogeneity of assimilated data sources. Therefore, the performance of this method  
380 should be evaluated in other mountain catchments. Recent remote sensing methods to retrieve snow depth from very high  
381 resolution stereoscopic imagery will be useful for that perspective. To further reduce the errors in the simulation at finer  
382 resolution, we also intend to add a data assimilation module in order to take advantage of other global datasets such as the  
383 snow cover area from remote sensing.

## 384 **Competing Interest**

385 Co-authors KB was a member of the NASA ASO team (which produced the lidar data used in this study). KB is currently  
386 employed by ASO, Inc., formed as a result of the ASO NASA technology transition effort.

## 387 **Acknowledgements**

388 We sincerely thank G. Liston for sharing the SnowModel code. We thank Franziska Koch and Olivier Merlin for fruitful  
389 discussions about this work.

390

## 391 **Code Availability**

392 The wrapper around the SnowModel code can be found here : SOURP Laura / ERA\_SnowModel\_Pipeline · GitLab:  
393 [https://src.koda.cnrs.fr/laura.sourp.1/era\\_snowmodel\\_pipeline](https://src.koda.cnrs.fr/laura.sourp.1/era_snowmodel_pipeline), last access: 15 March 2024.

395 **References**

- 396 Copernicus Digital Elevation Model: <https://spacedata.copernicus.eu/collections/copernicus-digital-elevation-model>, last  
397 access: 9 October 2023.
- 398 Retrieving data — Climate Data Store Toolbox 1.1.5 documentation: [https://cds.climate.copernicus.eu/toolbox/doc/how-](https://cds.climate.copernicus.eu/toolbox/doc/how-to/1_how_to_retrieve_data/1_how_to_retrieve_data.html)  
399 [to/1\\_how\\_to\\_retrieve\\_data/1\\_how\\_to\\_retrieve\\_data.html](https://cds.climate.copernicus.eu/toolbox/doc/how-to/1_how_to_retrieve_data/1_how_to_retrieve_data.html), last access: 27 June 2024.
- 400 Armstrong, R. L., Rittger, K., Brodzik, M. J., Racoviteanu, A., Barrett, A. P., Khalsa, S.-J. S., Raup, B., Hill, A. F., Khan, A.  
401 L., Wilson, A. M., Kayastha, R. B., Fetterer, F., and Armstrong, B.: Runoff from glacier ice and seasonal snow in High Asia:  
402 separating melt water sources in river flow, *Reg. Environ. Change*, <https://doi.org/10.1007/s10113-018-1429-0>, 2018.
- 403 Baba, M. W., Gascoïn, S., Jarlan, L., Simonneaux, V., and Hanich, L.: Variations of the Snow Water Equivalent in the Ourika  
404 Catchment (Morocco) over 2000–2018 Using Downscaled MERRA-2 Data, *Water*, 10, 1120,  
405 <https://doi.org/10.3390/w10091120>, 2018.
- 406 Baba, M. W., Gascoïn, S., Kinnard, C., Marchane, A., and Hanich, L.: Effect of Digital Elevation Model Resolution on the  
407 Simulation of the Snow Cover Evolution in the High Atlas, *Water Resour. Res.*, 55, 5360–5378,  
408 <https://doi.org/10.1029/2018WR023789>, 2019.
- 409 Baba, M. W., Boudhar, A., Gascoïn, S., Hanich, L., Marchane, A., and Chehbouni, A.: Assessment of MERRA-2 and ERA5  
410 to Model the Snow Water Equivalent in the High Atlas (1981–2019), *Water*, 13, 890, <https://doi.org/10.3390/w13070890>,  
411 2021.
- 412 Bair, E. H., Dozier, J., Rittger, K., Stillinger, T., Kleiber, W., and Davis, R. E.: How do tradeoffs in satellite spatial and  
413 temporal resolution impact snow water equivalent reconstruction?, *The Cryosphere*, 17, 2629–2643, [https://doi.org/10.5194/tc-](https://doi.org/10.5194/tc-17-2629-2023)  
414 [17-2629-2023](https://doi.org/10.5194/tc-17-2629-2023), 2023.
- 415 Bell, B., Hersbach, H., Simmons, A., Berrisford, P., Dahlgren, P., Horányi, A., Muñoz-Sabater, J., Nicolas, J., Radu, R.,  
416 Schepers, D., Soci, C., Villaume, S., Bidlot, J.-R., Haimberger, L., Woollen, J., Buontempo, C., and Thépaut, J.-N.: The ERA5  
417 global reanalysis: Preliminary extension to 1950, *Q. J. R. Meteorol. Soc.*, 147, 4186–4227, <https://doi.org/10.1002/qj.4174>,  
418 2021.
- 419 Bengtsson, L., Hagemann, S., and Hodges, K. I.: Can climate trends be calculated from reanalysis data?, *J. Geophys. Res.*  
420 *Atmospheres*, 109, <https://doi.org/10.1029/2004JD004536>, 2004.
- 421 Billecocq, P., Langlois, A., and Montpetit, B.: Subgridding High Resolution Numerical Weather Forecast in the Canadian  
422 Selkirk range for local snow modelling in a remote sensing perspective, *EGUsphere*, 1–24, [https://doi.org/10.5194/egusphere-](https://doi.org/10.5194/egusphere-2023-1152)  
423 [2023-1152](https://doi.org/10.5194/egusphere-2023-1152), 2023.
- 424 Bormann, K. J., Westra, S., Evans, J. P., and McCabe, M. F.: Spatial and temporal variability in seasonal snow density, *J.*  
425 *Hydrol.*, 484, 63–73, <https://doi.org/10.1016/j.jhydrol.2013.01.032>, 2013.

426 Broxton, P., Ehsani, M. R., and Behrangi, A.: Improving Mountain Snowpack Estimation Using Machine Learning With  
427 Sentinel-1, the Airborne Snow Observatory, and University of Arizona Snowpack Data, *Earth and Space Science*, 11,  
428 e2023EA002964, <https://doi.org/10.1029/2023EA002964>, 2024.

429 Buchhorn, M., Smets, B., Bertels, L., Roo, B. D., Lesiv, M., Tsendbazar, N.-E., Herold, M., and Fritz, S.: Copernicus Global  
430 Land Service: Land Cover 100m: collection 3: epoch 2019: Globe (V3.0.1), <https://doi.org/10.5281/zenodo.3939050>, 2020.

431 Buck, A. L.: New Equations for Computing Vapor Pressure and Enhancement Factor, *J. Appl. Meteorol. Climatol.*, 20, 1527–  
432 1532, [https://doi.org/10.1175/1520-0450\(1981\)020<1527:NEFCVP>2.0.CO;2](https://doi.org/10.1175/1520-0450(1981)020<1527:NEFCVP>2.0.CO;2), 1981.

433 C-SNOW: <https://ees.kuleuven.be/project/c-snow>, last access: 21 November 2024.

434 Deschamps-Berger, C., Gascoïn, S., Shean, D., Besso, H., Guiot, A., and López-Moreno, J. I.: Evaluation of snow depth  
435 retrievals from ICESat-2 using airborne laser-scanning data, *The Cryosphere*, 17, 2779–2792, <https://doi.org/10.5194/tc-17-2779-2023>, 2023.

437 Dumont, M., Tuzet, F., Gascoïn, S., Picard, G., Kutuzov, S., Lafaysse, M., Cluzet, B., Nheili, R., and Painter, T. H.: Accelerated  
438 Snow Melt in the Russian Caucasus Mountains After the Saharan Dust Outbreak in March 2018, *Journal of Geophysical  
439 Research: Earth Surface*, 125, <https://doi.org/10.1029/2020JF005641>, 2020.

440 Dutra, E., Muñoz-Sabater, J., Boussetta, S., Komori, T., Hirahara, S., and Balsamo, G.: Environmental Lapse Rate for High-  
441 Resolution Land Surface Downscaling: An Application to ERA5, *Earth Space Sci.*, 7, e2019EA000984,  
442 <https://doi.org/10.1029/2019EA000984>, 2020.

443 Fayad, A., Gascoïn, S., Faour, G., López-Moreno, J. I., Drapeau, L., Page, M. L., and Escadafal, R.: Snow hydrology in  
444 Mediterranean mountain regions: A review, *J. Hydrol.*, 551, 374–396, <https://doi.org/10.1016/j.jhydrol.2017.05.063>, 2017.

445 Freudiger, D., Kohn, I., Seibert, J., Stahl, K., and Weiler, M.: Snow redistribution for the hydrological modeling of alpine  
446 catchments, *Wiley Interdiscip. Rev. Water*, 4, e1232, <https://doi.org/10.1002/wat2.1232>, 2017.

447 GDAL/OGR contributors: GDAL/OGR Geospatial Data Abstraction software Library, Open Source Geospatial Foundation,  
448 <https://doi.org/10.5281/zenodo.5884351>, 2024.

449 Griffin, D. and Anchukaitis, K. J.: How unusual is the 2012–2014 California drought?, *Geophys. Res. Lett.*, 41, 9017–9023,  
450 <https://doi.org/10.1002/2014GL062433>, 2014.

451 Günther, D., Marke, T., Essery, R., and Strasser, U.: Uncertainties in Snowpack Simulations—Assessing the Impact of Model  
452 Structure, Parameter Choice, and Forcing Data Error on Point-Scale Energy Balance Snow Model Performance, *Water Resour.  
453 Res.*, 55, 2779–2800, <https://doi.org/10.1029/2018WR023403>, 2019.

454 Guyennon, N., Valt, M., Salerno, F., Petrangeli, A. B., and Romano, E.: Estimating the snow water equivalent from snow  
455 depth measurements in the Italian Alps, *Cold Reg. Sci. Technol.*, 167, 102859,  
456 <https://doi.org/10.1016/j.coldregions.2019.102859>, 2019.

457 Hersbach, H., Bell, B., Berrisford, P., Hirahara, S., Horányi, A., Muñoz-Sabater, J., Nicolas, J., Peubey, C., Radu, R., Schepers,  
458 D., Simmons, A., Soci, C., Abdalla, S., Abellan, X., Balsamo, G., Bechtold, P., Biavati, G., Bidlot, J., Bonavita, M., De Chiara,  
459 G., Dahlgren, P., Dee, D., Diamantakis, M., Dragani, R., Flemming, J., Forbes, R., Fuentes, M., Geer, A., Haimberger, L.,

460 Healy, S., Hogan, R. J., Hólm, E., Janisková, M., Keeley, S., Laloyaux, P., Lopez, P., Lupu, C., Radnoti, G., de Rosnay, P.,  
461 Rozum, I., Vamborg, F., Villaume, S., and Thépaut, J.-N.: The ERA5 global reanalysis, *Q. J. R. Meteorol. Soc.*, 146, 1999–  
462 2049, <https://doi.org/10.1002/qj.3803>, 2020.

463 Hoppinen, Z., Palomaki, R. T., Brencher, G., Dunmire, D., Gagliano, E., Marziliano, A., Tarricone, J., and Marshall, H.-P.:  
464 Evaluating Snow Depth Retrievals from Sentinel-1 Volume Scattering over NASA SnowEx Sites, *EGUsphere*, 1–35,  
465 <https://doi.org/10.5194/egusphere-2024-1018>, 2024.

466 Lievens, H., Demuzere, M., Marshall, H.-P., Reichle, R. H., Brucker, L., Brangers, I., de Rosnay, P., Dumont, M., Giroto, M.,  
467 Immerzeel, W. W., Jonas, T., Kim, E. J., Koch, I., Marty, C., Saloranta, T., Schöber, J., and De Lannoy, G. J. M.: Snow depth  
468 variability in the Northern Hemisphere mountains observed from space, *Nat. Commun.*, 10, 4629,  
469 <https://doi.org/10.1038/s41467-019-12566-y>, 2019.

470 Lievens, H., Brangers, I., Marshall, H.-P., Jonas, T., Olefs, M., and De Lannoy, G.: Sentinel-1 snow depth retrieval at sub-  
471 kilometer resolution over the European Alps, *The Cryosphere*, 16, 159–177, <https://doi.org/10.5194/tc-16-159-2022>, 2022.

472 Liston, G. E. and Elder, K.: A Distributed Snow-Evolution Modeling System (SnowModel), *J. Hydrometeorol.*, 7, 1259–1276,  
473 <https://doi.org/10.1175/JHM548.1>, 2006a.

474 Liston, G. E. and Elder, K.: A Meteorological Distribution System for High-Resolution Terrestrial Modeling (MicroMet), *J.*  
475 *Hydrometeorol.*, 7, 217–234, <https://doi.org/10.1175/JHM486.1>, 2006b.

476 Liston, G. E., Haeffel, R. B., Sturm, M., Hiemstra, C. A., Berezovskaya, S., and Tabler, R. D.: Simulating complex snow  
477 distributions in windy environments using SnowTran-3D, *J. Glaciol.*, 53, 241–256,  
478 <https://doi.org/10.3189/172756507782202865>, 2007.

479 Liston, G. E., Itkin, P., Stroeve, J., Tschudi, M., Stewart, J. S., Pedersen, S. H., Reinking, A. K., and Elder, K.: A Lagrangian  
480 Snow-Evolution System for Sea-Ice Applications (SnowModel-LG): Part I—Model Description, *J. Geophys. Res. Oceans*,  
481 125, e2019JC015913, <https://doi.org/10.1029/2019JC015913>, 2020.

482 Liu, Y., Fang, Y., Li, D., and Margulis, S. A.: How Well do Global Snow Products Characterize Snow Storage in High  
483 Mountain Asia?, *Geophys. Res. Lett.*, 49, e2022GL100082, <https://doi.org/10.1029/2022GL100082>, 2022.

484 López-Moreno, J. I., Fassnacht, S. R., Heath, J. T., Musselman, K. N., Revuelto, J., Latron, J., Morán-Tejeda, E., and Jonas,  
485 T.: Small scale spatial variability of snow density and depth over complex alpine terrain: Implications for estimating snow  
486 water equivalent, *Adv. Water Resour.*, 55, 40–52, <https://doi.org/10.1016/j.advwatres.2012.08.010>, 2013.

487 Mankin, J. S., Viviroli, D., Singh, D., Hoekstra, A. Y., and Diffenbaugh, N. S.: The potential for snow to supply human water  
488 demand in the present and future, *Environ. Res. Lett.*, 10, 114016, <https://doi.org/10.1088/1748-9326/10/11/114016>, 2015.

489 Marti, R., Gascoin, S., Berthier, E., de Pinel, M., Houet, T., and Laffly, D.: Mapping snow depth in open alpine terrain from  
490 stereo satellite imagery, *The Cryosphere*, 10, 1361–1380, <https://doi.org/10.5194/tc-10-1361-2016>, 2016.

491 Mernild, S. H., Liston, G. E., Hiemstra, C. A., Malmros, J. K., Yde, J. C., and McPhee, J.: The Andes Cordillera. Part I: snow  
492 distribution, properties, and trends (1979–2014), *Int. J. Climatol.*, 37, 1680–1698, <https://doi.org/10.1002/joc.4804>, 2017.

493 Mortimer, C., Mudryk, L., Cho, E., Derksen, C., Brady, M., and Vuyvich, C.: Use of multiple reference data sources to cross  
494 validate gridded snow water equivalent products over North America, *EGUsphere*, 1–31, [https://doi.org/10.5194/egusphere-](https://doi.org/10.5194/egusphere-2023-3013)  
495 2023-3013, 2024.

496 Mower, R., Gutmann, E. D., Lundquist, J., Liston, G. E., and Rasmussen, S.: Parallel SnowModel (v1.0): a parallel  
497 implementation of a Distributed Snow-Evolution Modeling System (SnowModel), *EGUsphere*, 1–27,  
498 <https://doi.org/10.5194/egusphere-2023-1612>, 2023.

499 Muñoz Sabater, J.: ERA5-Land hourly data from 1950 to present, <https://doi.org/10.24381/cds.e2161bac>, 2019.

500 Muñoz-Sabater, J., Dutra, E., Agustí-Panareda, A., Albergel, C., Arduini, G., Balsamo, G., Boussetta, S., Choulga, M.,  
501 Harrigan, S., Hersbach, H., Martens, B., Miralles, D. G., Piles, M., Rodríguez-Fernández, N. J., Zsoter, E., Buontempo, C.,  
502 and Thépaut, J.-N.: ERA5-Land: a state-of-the-art global reanalysis dataset for land applications, *Earth Syst. Sci. Data*, 13,  
503 4349–4383, <https://doi.org/10.5194/essd-13-4349-2021>, 2021.

504 Painter, T. H., Berisford, D. F., Boardman, J. W., Bormann, K. J., Deems, J. S., Gehrke, F., Hedrick, A., Joyce, M., Laidlaw,  
505 R., Marks, D., Mattmann, C., McGurk, B., Ramirez, P., Richardson, M., Skiles, S. M., Seidel, F. C., and Winstral, A.: The  
506 Airborne Snow Observatory: Fusion of scanning lidar, imaging spectrometer, and physically-based modeling for mapping  
507 snow water equivalent and snow albedo, *Remote Sens. Environ.*, 184, 139–152, <https://doi.org/10.1016/j.rse.2016.06.018>,  
508 2016.

509 Painter, T. H., Bormann, K., Deems, J. S., Hedrick, A. R., Marks, D. G., Skiles, M., and Stock, G. M.: Through the Looking  
510 Glass: Droughtorama to Snowpocalypse in the Sierra Nevada as studied with the NASA Airborne Snow Observatory, 2017,  
511 C12C-08, 2017.

512 Quéno, L., Mott, R., Morin, P., Cluzet, B., Mazzotti, G., and Jonas, T.: Snow redistribution in an intermediate-complexity  
513 snow hydrology modelling framework, *EGUsphere*, 1–32, <https://doi.org/10.5194/egusphere-2023-2071>, 2023.

514 Raleigh, M. S., Livneh, B., Lapo, K., and Lundquist, J. D.: How Does Availability of Meteorological Forcing Data Impact  
515 Physically Based Snowpack Simulations?, *J. Hydrometeorol.*, 17, 99–120, <https://doi.org/10.1175/JHM-D-14-0235.1>, 2016.

516 Raleigh, M. S. and Small, E. E.: Snowpack density modeling is the primary source of uncertainty when mapping basin-wide  
517 SWE with lidar, *Geophysical Research Letters*, 44, 3700–3709, <https://doi.org/10.1002/2016GL071999>, 2017.

518 Shao, D., Li, H., Wang, J., Hao, X., Che, T., and Ji, W.: Reconstruction of a daily gridded snow water equivalent product for  
519 the land region above 45° N based on a ridge regression machine learning approach, *Earth Syst. Sci. Data*, 14, 795–809,  
520 <https://doi.org/10.5194/essd-14-795-2022>, 2022.

521 Skiles, S. M., Flanner, M., Cook, J. M., Dumont, M., and Painter, T. H.: Radiative forcing by light-absorbing particles in snow,  
522 *Nature Clim Change*, 8, 964–971, <https://doi.org/10.1038/s41558-018-0296-5>, 2018.

523 Sturm, M., Taras, B., Liston, G. E., Derksen, C., Jonas, T., and Lea, J.: Estimating Snow Water Equivalent Using Snow Depth  
524 Data and Climate Classes, *J. Hydrometeorol.*, 11, 1380–1394, <https://doi.org/10.1175/2010JHM1202.1>, 2010.

525 Sturm, M., Goldstein, M. A., and Parr, C.: Water and life from snow: A trillion dollar science question: SNOW AND LIFE,  
526 *Water Resour. Res.*, 53, 3534–3544, <https://doi.org/10.1002/2017WR020840>, 2017.

527 Tsai, Y.-L. S., Dietz, A., Oppelt, N., and Kuenzer, C.: Remote Sensing of Snow Cover Using Spaceborne SAR: A Review,  
528 Remote Sens., 11, 1456, <https://doi.org/10.3390/rs11121456>, 2019.

529 Urraca, R. and Gobron, N.: Temporal stability of long-term satellite and reanalysis products to monitor snow cover trends, The  
530 Cryosphere, 17, 1023–1052, <https://doi.org/10.5194/tc-17-1023-2023>, 2023.

531 Viviroli, D., Kumm, M., Meybeck, M., Kallio, M., and Wada, Y.: Increasing dependence of lowland populations on mountain  
532 water resources, Nat. Sustain., 3, 917–928, <https://doi.org/10.1038/s41893-020-0559-9>, 2020.

533 Weber, M., Koch, F., Bernhardt, M., and Schulz, K.: The evaluation of the potential of global data products for snow  
534 hydrological modelling in ungauged high-alpine catchments, Hydrol. Earth Syst. Sci., 25, 2869–2894,  
535 <https://doi.org/10.5194/hess-25-2869-2021>, 2021.

536 WMO e-Library: <https://library.wmo.int/idurl/4/58104>, last access: 15 March 2024.

537 Wrzesien, M. L., Pavelsky, T. M., Durand, M. T., Dozier, J., and Lundquist, J. D.: Characterizing Biases in Mountain Snow  
538 Accumulation From Global Data Sets, Water Resour. Res., 55, 9873–9891, <https://doi.org/10.1029/2019WR025350>, 2019.

539

540

Copernicus class number	Copernicus Vegetation type	Forest type	Leaf type	Chosen corresponding SM class	SM class number
0	Nodata				-9999
20	Shrubs			Mesic upland shrub	6
30	Herbaceous Vegetation			Grassland rangeland	12
40	cropland			short crops	23
50	Urban			Residential/urban	21
60	sparse vegetation			Bare	18
70	Snow and ice			Permanent snow/glacier	20
80	Permanent water bodies			water/ possibly frozen	19
90	Herbaceous wetland			Shrub wetland/ riparian	9
100	Moss and lichen			Bare	18
111	closed forest	evergreen	needle	Coniferous forest	1
112	closed forest	evergreen	broad	Coniferous forest	1
113	closed forest	deciduous	needle	Deciduous forest	2

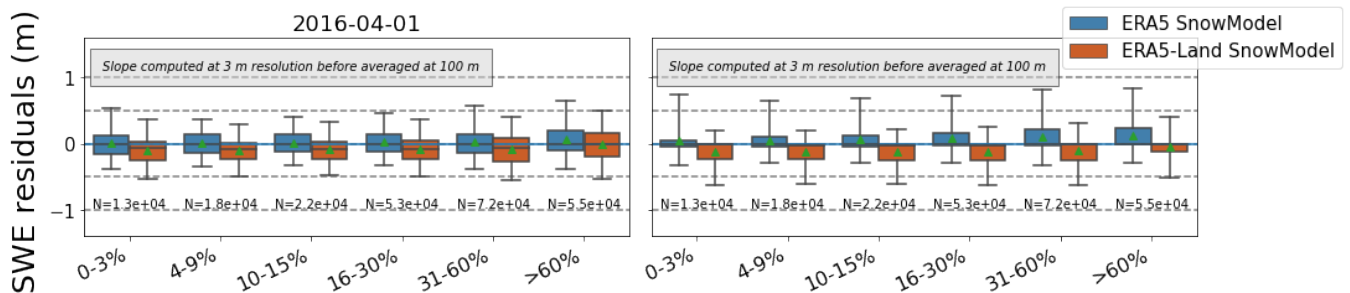
114	closed forest	deciduous	broad	Deciduous forest	2
115	closed forest	mixed		Mixed forest	3
116	closed forest	unknown		Mixed forest	3
121	open forest	evergreen	needle	Coniferous forest	1
122	open forest	evergreen	broad	Coniferous forest	1
123	open forest	deciduous	needle	Deciduous forest	2
124	open forest	deciduous	broad	Deciduous forest	2
125	open forest	mixed		Mixed forest	3
126	open forest	unknown		Mixed forest	3
200	open sea			Ocean	24

542

543

**Table A1 : Correspondence table between Copernicus land cover and SnowModel vegetation classes**

544



545

546

**Figure A2: Distribution of the residuals between the SnowModel simulated SWE and the ASO SWE at 100 m resolution in the Tuolumne river catchment (in m w.e.) on the 1st of April 2016 (left) and the 27th of May (right), stratified by**

547



548 **slope. Whiskers show the 5-95 percentile, the line in each box represents the median of the distribution and the green**  
549 **triangle shows the mean. Slope has been calculated using the DEM at 3 m resolution and has been resampled with an**  
550 **average algorithm at 100 m.**